Letter

Symmetry constraints and spectral crossing in a Mott insulator with Green's function zeros

Chandan Setty,[1,*,†] Shouvik Sur,[1,*,‡] Lei Chen,[1] Fang Xie,[1] Haoyu Hu,[1,2] Silke Paschen,[1,3] Jennifer Cano,[4,5] and Qimiao Si[1]

[1]*Department of Physics and Astronomy, Rice Center for Quantum Materials, Rice University, Houston, Texas 77005, USA*
[2]*Donostia International Physics Center, P. Manuel de Lardizabal 4, 20018 Donostia-San Sebastian, Spain*
[3]*Institute of Solid State Physics, Vienna University of Technology, Wiedner Hauptstr. 8-10, 1040, Vienna, Austria*
[4]*Department of Physics and Astronomy, Stony Brook University, Stony Brook, New York 11794, USA*
[5]*Center for Computational Quantum Physics, Flatiron Institute, New York, New York 10010, USA*

(Received 6 March 2023; accepted 29 May 2024; published 26 July 2024)

Lattice symmetries are central to the characterization of electronic topology. Recently, it was shown that Green's function eigenvectors form a representation of the space group. This formulation has allowed the identification of gapless topological states even when quasiparticles are absent. Here we demonstrate the profundity of the framework in the extreme case, when interactions lead to a Mott insulator, through a solvable model with long-range interactions. We find that both Mott poles and zeros are subject to the symmetry constraints, and relate the symmetry-enforced spectral crossings to degeneracies of the original noninteracting eigenstates. Our results lead to new understandings of topological quantum materials and highlight the utility of interacting Green's functions toward their symmetry-based design.

DOI: 10.1103/PhysRevResearch.6.L032018

Introduction. In band theory of noninteracting topological semimetals, lattice symmetries act as indicators of topology and have been widely exploited in identifying novel topological materials [1–7]. The effects of interactions in topological semimetals are typically analyzed perturbatively [1,8–15]. Interacting systems have also been treated approximately in terms of renormalized noninteracting Hamiltonians (the so called topological Hamiltonians) [16,17], where lattice symmetries can constrain single particle [18] and collective [19] excitations. To address the interplay between strong correlations and topology, however, nonperturbative approaches to the interactions are required. Whether and how symmetry constraints operate is *a priori* unclear, especially when the interaction terms in a Hamiltonian do not commute with the single-particle terms.

Recently, a group that includes several of us have shown that the Green's function eigenvectors form a representation of the space group [20]. Symmetry enforced or protected degeneracies then respectively follow when the dimensionality of irreducible representation is greater than one at a given high symmetry point, or when two irreducible representations with distinct symmetry eigenvalues cross along a high symmetry line. This formulation was applied to the case of a multichannel Kondo lattice, which describes a non-Fermi liquid metal with dispersive modes arising from fractionalized electronic excitations. The eigenvectors of the Green's function were used to define degeneracies by locating spectral crossings [20]. The approach also provided the theoretical basis for the robustness [21] of Kondo-driven Weyl semimetals [22–24].

The extreme form of correlation effects occurs when the interactions drive a metal into a Mott localized state. It is an intriguing question as to what role topological nodes of the noninteracting limit may have in Mott insulators [25]. Along this direction, determining how symmetry constraints operate in a Mott insulator represents an outstanding open question. One of the important features of a Mott insulator is that it can have Green's function poles and zeros, both of which contribute to the Luttinger count of electronic states [26]. Does symmetry constrain both features?

In this work, we address the symmetry constraints of a Mott insulator using the Green's function approach [20]. To be specific, we present our analysis on a lattice model in which the noninteracting Hamiltonian has symmetry-enforced Dirac nodes, though we expect our results to be valid more generally. Importantly, the symmetry constrains the Green's functions at all frequencies and the degeneracies at the high symmetry wave vectors appear in the form of spectral crossings; in particular, we find that this operates on both Green's function poles and zeros. Our qualitative results are illustrated in Fig. 1: the spectral crossings of the Green's function poles [(c)] and Green's function zeros [(d)] appears as the wave vector moves [(b)] toward the high symmetry wave vector P; this captures the degeneracy of the Green's function eigenvectors at P, where the Bloch functions of the noninteracting counterpart are degenerate [(a), top panel]. They give rise

*These authors contributed equally to this work.
†Contact author: csetty@rice.edu
‡Contact author: shouvik.sur@rice.edu

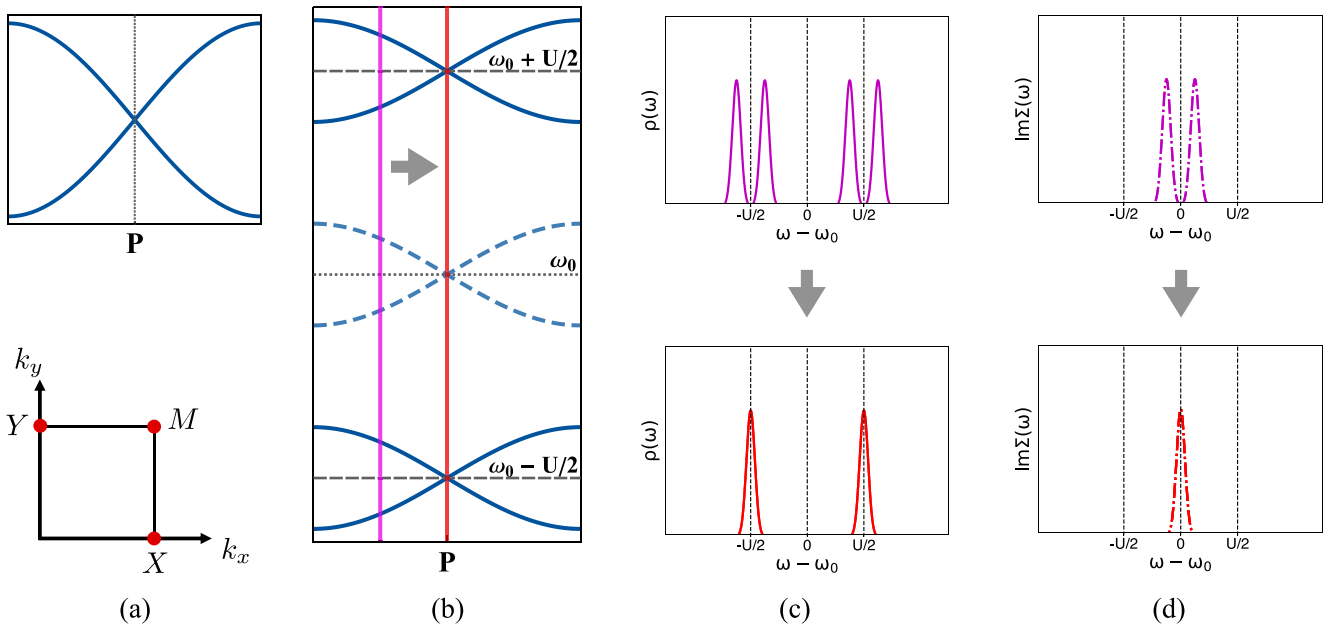

FIG. 1. Schematic summary of symmetry constraints and spectral crossings in a Mott insulator with Green's functions zeros and poles. (a) Top: Symmetry enforced Dirac point in the noninteracting dispersion that occurs at a high symmetry point P. Bottom: Dirac points (red dots) that occur in the square net lattice at high symmetry points in the Brillouin zone. (b) Symmetry enforced spectral crossings in the Mott insulator state. They involve the upper and lower Hubbard bands (solid curves) and their associated Dirac points are separated by U and a contour of crossings of zeros (dashed curves). Both are enforced by the lattice symmetry. (c) Top: Spectral function (imaginary part of the Green's function) at a wave vector marked by the magenta line in (b) away from the Dirac point for the poles of the Green's function. Bottom: Spectral function at the wave vector P marked by the red line in (b) at the Dirac point. (d) Top: Imaginary part of the self energy at a wave vector marked by the magenta line in (b) indicating zeros of the Green's function. Bottom: Same at the wave vector P marked by the red line indicating degeneracies of zeros enforced by symmetry.

to new understandings of topological quantum materials and set the stage for systematic analysis of the topology of Mott insulators.

Interacting square net lattice and solution method. We consider a two-dimensional (2D) square net lattice, as illustrated in Fig. 1 in the Supplemental Material (SM) [27]. Here, the noninteracting bands contain symmetry enforced Dirac crossings at the X and M points in the Brillouin zone [Fig. 1(a), bottom panel] [28]. We focus on local in momentum interactions analogous to those appearing in the Hatsugai-Kohmoto (HK) model [25,29–38]. This form of interaction can be solved exactly (see the SM [27], Sec. III), which facilitates the understanding of not only the symmetry-enforced spectral crossing but also the symmetry constraints on dispersive poles and zeros as we do below.

The Hamiltonian of a 2D square net lattice (see SM [27]) in the orbital basis $\Lambda_{\boldsymbol{k}}^{\intercal} \equiv (c_{A,\Uparrow}, c_{A,\Downarrow}, c_{B,\Uparrow}, c_{B,\Downarrow})_{\boldsymbol{k}}$ takes the form $\tilde{\mathscr{H}} = \tilde{\mathscr{H}}_0 + \tilde{\mathscr{H}}_I$, where

$$\begin{aligned}\tilde{\mathscr{H}}_0 &= \sum_{\boldsymbol{k}} \Lambda_{\boldsymbol{k}}^{\dagger} \tilde{h}_0(\boldsymbol{k}) \Lambda_{\boldsymbol{k}} \\ \tilde{\mathscr{H}}_I &= \frac{\alpha}{2} \sum_{\boldsymbol{k}} \Lambda_{\boldsymbol{k}}^{\dagger} \Lambda_{\boldsymbol{k}} + \frac{U_c}{2} \sum_{\boldsymbol{k}} (\Lambda_{\boldsymbol{k}}^{\dagger} \Lambda_{\boldsymbol{k}})^2 \\ &\quad + \frac{U_s}{2} \sum_{\boldsymbol{k}} (\Lambda_{\boldsymbol{k}}^{\dagger} \tau_1 \otimes \sigma_0 \Lambda_{\boldsymbol{k}})^2, \end{aligned} \tag{1}$$

with $\tilde{h}_0(\boldsymbol{k}) = t_2(\cos k_x + \cos k_y)\mathbb{1} + 2t \cos \frac{k_x}{2} \cos \frac{k_y}{2} \tau_1 \otimes \sigma_0 + t_{SO}[\sin k_x \tau_3 \otimes \sigma_2 - \sin k_y \tau_3 \otimes \sigma_1] - \mu \mathbb{1}$, τ_j (σ_j) being the jth Pauli matrix acting on the sublattice (spin) subspace, and $\mathbb{1}$ is the 4×4 identity matrix. Here, $c_{a,b}$ are the annihilation operators for electrons in the original sublattice $a = A, B$ and physical spin $b = \Uparrow, \Downarrow$ indices. t, t_2 are the hopping parameters, t_{SO} is the spin-orbit coupling, U_c and U_s are intra and interorbital interaction, respectively, and α is a constant shift in the density which we fix to $-(U_c + U_s)$ for convenience. As we shall show below, a finite U_s introduces an asymmetry between the dispersion of the poles and zeros of the interacting Greens function, which is expected in a generic interacting system. Without loss of generality, henceforth, we set $t_2 = 0$; the noninteracting bandwidth is $8t$.

It is convenient to work in a basis where the noninteracting Hamiltonian is block diagonal. To this end, we rotate the original basis of $\Lambda_{\boldsymbol{k}}^{\intercal}$ into the new basis $\Phi_{\boldsymbol{k}}^{\intercal} \equiv (\phi_{+,\Uparrow}, \phi_{+,\Downarrow}, \phi_{-,\Uparrow}, \phi_{-,\Downarrow})_{\boldsymbol{k}} \equiv \frac{1}{\sqrt{2}}(c_{A,\Uparrow} + c_{B,\Uparrow}, c_{A,\Downarrow} - c_{B,\Downarrow}, -c_{A,\Uparrow} + c_{B,\Uparrow}, c_{A,\Downarrow} + c_{B,\Downarrow})_{\boldsymbol{k}}$. This amounts to block diagonalizing the Hamiltonian matrix as $\tilde{h}_0(\boldsymbol{k}) \to h_0(\boldsymbol{k}) = e^{i\frac{\pi}{4}\tau_2 \otimes \sigma_3} \tilde{h}_0(\boldsymbol{k}) e^{-i\frac{\pi}{4}\tau_2 \otimes \sigma_3}$, where $h_0(\boldsymbol{k}) = \vec{n}(\boldsymbol{k}) \cdot \vec{\Gamma} - \mu \mathbb{1}$ with $\vec{n}(\boldsymbol{k}) = \{-t_{SO} \sin k_y, t_{SO} \sin k_x, 2t \cos \frac{k_x}{2} \cos \frac{k_y}{2}\}$ and $\vec{\Gamma} = \tau_3 \otimes \vec{\sigma}$. It supports doubly degenerate bands which disperse as $\tilde{\xi}_j = -\mu + (-1)^j |\vec{n}(\boldsymbol{k})|$. In the $\Phi_{\boldsymbol{k}}$ basis,

$$\begin{aligned}\tilde{\mathscr{H}}_I \to \mathscr{H}_I &= \frac{U_c}{2} \sum_{\boldsymbol{k}} (\Phi_{\boldsymbol{k}}^{\dagger} \Phi_{\boldsymbol{k}})^2 + \frac{\alpha}{2} \sum_{\boldsymbol{k}} \Phi_{\boldsymbol{k}}^{\dagger} \Phi_{\boldsymbol{k}} \\ &\quad + \frac{U_s}{2} \sum_{\boldsymbol{k}} (\Phi_{\boldsymbol{k}}^{\dagger} \tau_3 \otimes \sigma_3 \Phi_{\boldsymbol{k}})^2. \end{aligned} \tag{2}$$

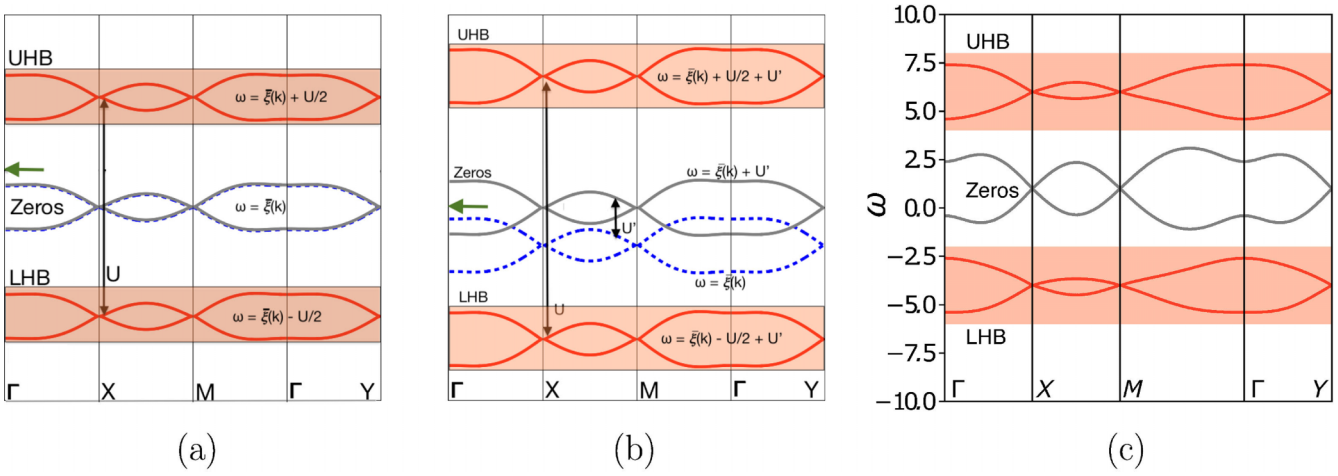

FIG. 2. Exact poles and zeros of the total Green's function of an interacting Dirac semimetal as $\beta \to \infty$. (a) The upper and lower Hubbard bands (red curves marked UHB and LHB, respectively) and zeros (gray) obtained from analytical diagonalization of the interacting Hamiltonian in the $t_{SO}/t \ll 1$ limit at $U' = 0$. The blue dotted curve is the original noninteracting band structure which transforms to zeros at sufficiently strong U. The green arrow marks the chemical potential. (b) Same as (a) but for $U' > 0$. Here the contours of zeros and poles are shifted by U'. (c) The spectrum of the Green's function obtained by numerical exact diagonalization of the interacting Hamiltonian with $(t, t_{SO}, \mu) = (0.7, 0.42, 5)$ and $(U, U') = (10, 0.5)$.

Here $\Phi_{\boldsymbol{k}}^\dagger \Phi_{\boldsymbol{k}}$ is the total charge and $\Phi_{\boldsymbol{k}}^\dagger \tau_3 \otimes \sigma_3 \Phi_{\boldsymbol{k}}$ is a staggered pseudosublattice density for a given momentum.

In the band basis, $\Psi_{\boldsymbol{k}} = (\psi_{1,\uparrow}, \psi_{1,\downarrow}, \psi_{2,\uparrow}, \psi_{2,\downarrow})_{\boldsymbol{k}}^\intercal$ with $\{\psi_{j,\uparrow}, \psi_{j,\downarrow}\}$ representing the jth pair of degenerate bands, h_0 is diagonalized to $[-\mu \mathbb{1} + |\vec{n}(\boldsymbol{k})| \tau_3 \otimes \sigma_0]$. Henceforth, we treat $\sigma = \uparrow, \downarrow$ and $i, j = 1, 2$ as pseudospin and band indices, respectively. In the limit of weak spin-orbit coupling, $(t_{SO}/t) \ll 1$, the total Hamiltonian can be cast into the form $H = H_0 + H_I$ with $H_0 = \sum_{\boldsymbol{k}i\sigma} \xi_{i\sigma}(\boldsymbol{k}) \psi_{i\sigma}^\dagger(\boldsymbol{k}) \psi_{i\sigma}(\boldsymbol{k})$ and

$$H_I = U \sum_{\boldsymbol{k}i} n_{\boldsymbol{k}i\uparrow} n_{\boldsymbol{k}i\downarrow} + U' \sum_{\substack{\boldsymbol{k}\sigma\sigma' \\ i \neq j}} n_{\boldsymbol{k}i\sigma} n_{\boldsymbol{k}j\sigma'} + \mathcal{O}(t_{SO}/t), \quad (3)$$

where $(U, U') = (U_c + U_s, U_c - U_s)$, and correspond to intraband and interband interactions, respectively. We utilize the density basis to exactly diagonalize the interacting Hamiltonian with interaction terms up to $\mathcal{O}(t_{SO}/t)^0$. The additional $\mathcal{O}(t_{SO}/t)^{n>0}$ terms only distort the bands keeping the degeneracies intact. A full numerical solution for $t \sim t_{SO}$ appears later in the main text and in the SM [27] (Sec. I). The renormalized band dispersions satisfy $\xi_{i\uparrow}(\boldsymbol{k}) = \xi_{i\downarrow}(\boldsymbol{k})$, and are related to the bare band dispersions, $\tilde{\xi}_i(\boldsymbol{k})$, as $\xi_i(\boldsymbol{k}) \equiv \tilde{\xi}_i(\boldsymbol{k}) - U/2$. The density operators of $\psi_{\boldsymbol{k}i\sigma}$ are denoted as $n_{\boldsymbol{k}i\sigma}$.

In the presence of time reversal symmetry, the total Green's function can be evaluated exactly as outlined in the SM [27] (Sec. II). The calculation captures Fig. 3 in the SM [27], which shows the transitions that contribute to the zero of the Green's function. It simplifies in the zero temperature limit ($\beta \to \infty$) where both $\xi_1(\boldsymbol{k}), \xi_2(\boldsymbol{k})$ are filled with $U, U' > 0$. Further, for each $\boldsymbol{k}$, when $U + 2U' > |\xi_1| + 2|\xi_2|, 2|\xi_1| + |\xi_2|$ and $U > 2|\xi_1|, 2|\xi_2|$ but $U' < |\xi_1| + |\xi_2|$, the partition function is $Z_{\boldsymbol{k}} = \lim_{\beta\to\infty} 4e^{-\beta(\xi_1+\xi_2+U')}$, and we obtain

$$G(z, \boldsymbol{k}) = \frac{1}{\tilde{G}^{-1}(z, \boldsymbol{k}) - (U/2)^2 \tilde{G}(z, \boldsymbol{k})} \quad (4)$$

in the orbital basis, where $\tilde{G}^{-1}(z, \boldsymbol{k}) = z\mathbb{1} - [\vec{n}(\boldsymbol{k}) \cdot \vec{\Gamma} - (\mu - U')\mathbb{1}]$. Thus, the net impact of interactions in Eq. (3) is to shift the chemical potential $\mu \to \mu - U'$, and generate the self energy,

$$\Sigma(z, \boldsymbol{k}) = (U/2)^2 \tilde{G}(z, \boldsymbol{k}). \quad (5)$$

The locations of poles and zeros of G on the complex-z plane are deduced from the roots of the denominator and numerator, respectively, of its determinant,

$$\det G(z, \boldsymbol{k}) = \frac{[(z + (\mu - U'))^2 - |\vec{n}(\boldsymbol{k})|^2]^2}{\left[(z + (\mu - U'))^2 - \left(\frac{U}{2} + |\vec{n}(\boldsymbol{k})|\right)^2\right]^2 \left[(z + (\mu - U'))^2 - \left(\frac{U}{2} - |\vec{n}(\boldsymbol{k})|\right)^2\right]^2}. \quad (6)$$

Green's function poles and zeros. When $U' = 0$, we have two decoupled copies of Dirac bands with only intraband interaction U. When both bands are below the chemical potential, we can treat the two bands separately and use the one band formula (Eq. (S17) in SM [27]) for the individual bands. The partition function is simply a product of that for the individual bands and is given by $Z = \prod_{\boldsymbol{k}} \prod_{i=i,2} Z_{\boldsymbol{k}i}$ with $Z_{\boldsymbol{k}i} = 1 + 2e^{-\beta\xi_i(\boldsymbol{k})} + e^{-\beta(2\xi_i(\boldsymbol{k})+U)}$. Each band is split into a lower and upper Hubbard band with a crossing of zeros at the energies of the original noninteracting bands. A schematic of the various crossings is shown in Fig. 2(a).

The spectral function of the interacting Dirac semimetal model at $U' \neq 0$ is shown in Fig. 2(b). The spectral functions are analogous to the case of $U' = 0$ but with the bands

shifted by U'. Additionally, the contour of zeros splits from the original noninteracting bands (dashed blue curves). The features of G obtained in the limit of weak spin-orbit coupling, $(t_{SO}/t) \ll 1$, persists at more generic values of (t_{SO}/t), as demonstrated by numerically diagonalizing the interacting Hamiltonian in Fig. 2(c).

Symmetry constraints and spectral crossings. The Green's function eigenvectors form a representation of the space group, as formulated in Ref. [20] (and briefly summarized in the SM [27], Sec. IV), and are expected to form fourfold degeneracies at the wave vectors X, Y, and M: As in the noninteracting case [28], the degeneracies at the X/Y points are protected by $\{M_z|\frac{1}{2}\frac{1}{2}\}$ nonsymmorphic mirror symmetry or $\{C_{2x}|\frac{1}{2}0\}/\{C_{2y}|0\frac{1}{2}\}$ nonsymmorphic screw-axis rotations, while those at the M point are also protected by the $\{C_{2x}|\frac{1}{2}0\}$ and $\{C_{2y}|0\frac{1}{2}\}$ nonsymmorphic rotations. Our results for all three cases, with $t_{SO}/t \ll 1$ and $U' = 0$ [Fig. 2(a)] and $U' \neq 0$ [Fig. 2(b)] as well as for the case of unconstrained ratio t_{SO}/t [Fig. 2(c)], demonstrate that the entire spectra obey such degeneracies. This is so even though the system is a Mott insulator with a spectral gap. Moreover, the spectral crossing also applies to the Green's function zeros. While for the cases (a) and (b), $G(z, \boldsymbol{k})$ is diagonal in the same basis that diagonalized the noninteracting Hamiltonian [see the SM [27] (Sec. V)], this special property does not apply to the case (c) nor to the other cases that we have analyzed [see the SM [27], Figs. 2(d) and 2(e)]. Our results, thus, illustrate our central point, namely the eigenvectors and eigenvalues of the Green's function can be used to define degeneracies by locating spectral crossings of strongly correlated systems. We note that in our model time-reversal symmetry protects the bands of zeros. In its absence, Green's function zeros may appear only at high-symmetry locations [25], but our conclusions continue to be applicable to the poles that constitute the Hubbard bands, as discussed in details in Sec. VI of the SM [27].

Discussion. Several remarks are in order. First, here we have considered the various cases of the interactions and demonstrated the existence of both poles and zeros of the interacting Green's function that cross at high-symmetry locations. These crossings are enforced by space group symmetries. For more generic interactions, we expect an extended regime of interactions where the Green's function zeros persist and the crossings of the poles and zeros continue to be enforced by lattice symmetries. In the SM [27], Sec. I, we have studied all possible symmetry allowed interaction terms for the square net lattice. We find our conclusions are robust as has been illustrated in Fig. 1. We note that in multiband systems a wide variety of interactions, such as those considered here, are present that involve couplings between various internal degrees of freedom, viz. orbitals, valleys, etc. [39,40]. Such terms go beyond the standard interaction in the Hubbard model, and find applicability in down-folded effective models [41]. For the case of zeros, we also explicitly demonstrate their symmetry-enforced crossings for Hubbard interactions via a cluster slave-spin calculation, as detailed in the Sec. VII of the SM [27]. Second, we have used both the Green's function poles and zeros to illustrate the point that the spectral crossings occur at distinct energies. That the crossings of various bands of poles and zeros can be treated separately, depending on the choice of frequency, highlights a distinct advantage of working with Green's function eigenvectors. We have also demonstrated the symmetry enforced crossings of zeros and poles in another lattice model (diamond lattice [42,43]) with HK interaction, which can be found in Sec. VIII in the SM [27]. Third, the kind of spectral crossings we have discussed sets the stage to analyze the form of topology when strong correlations turn a noninteracting topological semimetal into a Mott insulator. One way to define such topology is through a classification of the eigenvectors of the Green's function [20], which leads to frequency-dependent topological invariants, and associates a monopole charge to the crossings of the bands of zeros [44]. An additional outcome of this method is the elucidation of the manner in which the Green's function zeros may contribute to topological response in a Mott insulating state [45]. Finally, by demonstrating symmetry constraints and spectral crossing in an extreme interacting setting, our work provides support to the work of Ref. [20]. There, spectral crossings through symmetry constraints plays a central role in realizing topological semimetals without Landau quasiparticles.

Implications for experiments and materials. The Green's function eigenvector formulation [20] is expected to yield spectral crossings in other symmetry settings. For example, in the case of Bi_2CuO_4, an eightfold degeneracy [46] is expected at certain high symmetry wave vectors in its noninteracting bandstructure [47]. The system is in fact strongly interacting [48,49] and we expect that its paramagnetic Mott insulator state (above its Néel temperature of 50 K [50]) will feature eightfold spectral crossings in the form we have described in some detail here. Probing the spectral function by applying a symmetry-breaking perturbation will allow for experimentally revealing this spectral crossing.

Separately, proximity to an orbital-selective Mott insulating state has recently been advanced as a means of generating Kondo-driven topological semimetals in d-electron-based systems that host topological flat bands [51–53]. We can expect that the type of spectral crossings of both the peaks and zeros as discussed here may play an important role in such orbital-selective Mott states.

To conclude, we provide a proof-of-principle demonstration of how lattice symmetries can be used to constrain excitations in an extreme limit of strongly correlated systems. Typically in noninteracting systems, eigenstates of the Hamiltonian and their symmetry operators are used to indicate topology by diagnosing conditions for symmetry protected band crossings. For interacting systems, we recently showed that Green's function eigenvectors form a representation of the lattice space group and can be used to diagnose and realize topology [20]. Here we study an exactly solvable model of a Mott insulator where eigenvectors and eigenvalues of the Green's function can be used to locate crossings of poles and zeros in momentum space. Together with the realization of topological semimetals without Landau quasiparticles, our work demonstrates the power that the Green's function formulation of symmetry constraints displays for realizing nontrivial spectral crossings in fully interacting settings. We can expect the approach to be important for the symmetry-based design of topological quantum materials.

Note added: After the completion of this manuscript, a recent work addressing a different model with a focus on the Green's function zeros and poles in interacting topological insulators became available (N. Wagner *et al.* [54]).

Acknowledgments. We thank N. Nagaosa for a useful discussion. Work at Rice has primarily been supported by the National Science Foundation under Grant No. DMR-2220603 (F.X. and Q.S.), by the Air Force Office of Scientific Research under Grant No. FA9550-21-1-0356 (C.S. and S.S.), and by the Robert A. Welch Foundation Grant No. C-1411 (L.C.) and the Vannevar Bush Faculty Fellowship ONR-VB N00014-23-1-2870 (Q.S.). The majority of the computational calculations have been performed on the Shared University Grid at Rice funded by the NSF under Grant EIA-0216467, a partnership between Rice University, Sun Microsystems, and Sigma Solutions, Inc.; the Big-Data Private-Cloud Research Cyberinfrastructure MRI-award funded by the NSF under Grant No. CNS-1338099; and the Extreme Science and Engineering Discovery Environment (XSEDE) by the NSF under Grant No. DMR170109. H.H. acknowledges the support of the European Research Council (ERC) under the European Union's Horizon 2020 research and innovation program (Grant Agreement No. 101020833). Work in Vienna was supported by the Austrian Science Fund (Project I 5868-N - FOR 5249 - QUAST) and the ERC (Advanced Grant CorMeTop, No. 101055088). J.C. acknowledges the support of the National Science Foundation under Grant No. DMR-1942447, support from the Alfred P. Sloan Foundation through a Sloan Research Fellowship and the support of the Flatiron Institute, a division of the Simons Foundation. S.P. and Q.S. acknowledge the hospitality of the Aspen Center for Physics, which is supported by NSF Grant No. PHY-2210452.

[1] N. P. Armitage, E. J. Mele, and A. Vishwanath, Weyl and Dirac semimetals in three-dimensional solids, Rev. Mod. Phys. **90**, 015001 (2018).

[2] N. Nagaosa, T. Morimoto, and Y. Tokura, Transport, magnetic and optical properties of Weyl materials, Nat. Rev. Mater. **5**, 621 (2020).

[3] B. Bradlyn, L. Elcoro, J. Cano, M. G. Vergniory, Z. Wang, C. Felser, M. I. Aroyo, and B. A. Bernevig, Topological quantum chemistry, Nature (London) **547**, 298 (2017).

[4] J. Cano, B. Bradlyn, Z. Wang, L. Elcoro, M. G. Vergniory, C. Felser, M. I. Aroyo, and B. A. Bernevig, Building blocks of topological quantum chemistry: Elementary band representations, Phys. Rev. B **97**, 035139 (2018).

[5] H. C. Po, A. Vishwanath, and H. Watanabe, Symmetry-based indicators of band topology in the 230 space groups, Nat. Commun. **8**, 50 (2017).

[6] H. Watanabe, H. C. Po, M. P. Zaletel, and A. Vishwanath, Filling-enforced gaplessness in band structures of the 230 space groups, Phys. Rev. Lett. **117**, 096404 (2016).

[7] J. Cano and B. Bradlyn, Band representations and topological quantum chemistry, Annu. Rev. Condens. Matter Phys. **12**, 225 (2021).

[8] D. T. Son, Quantum critical point in graphene approached in the limit of infinitely strong Coulomb interaction, Phys. Rev. B **75**, 235423 (2007).

[9] K. Sun, H. Yao, E. Fradkin, and S. A. Kivelson, Topological insulators and nematic phases from spontaneous symmetry breaking in 2d Fermi systems with a quadratic band crossing, Phys. Rev. Lett. **103**, 046811 (2009).

[10] O. Vafek and K. Yang, Many-body instability of Coulomb interacting bilayer graphene: Renormalization group approach, Phys. Rev. B **81**, 041401(R) (2010).

[11] I. F. Herbut, V. Juričić, and B. Roy, Theory of interacting electrons on the honeycomb lattice, Phys. Rev. B **79**, 085116 (2009).

[12] S. Sur and R. Nandkishore, Instabilities of Weyl loop semimetals, New J. Phys. **18**, 115006 (2016).

[13] Y. Huh, E.-G. Moon, and Y. B. Kim, Long-range Coulomb interaction in nodal-ring semimetals, Phys. Rev. B **93**, 035138 (2016).

[14] B. Roy, Interacting nodal-line semimetal: Proximity effect and spontaneous symmetry breaking, Phys. Rev. B **96**, 041113(R) (2017).

[15] S. Sur and B. Roy, Unifying interacting nodal semimetals: A new route to strong coupling, Phys. Rev. Lett. **123**, 207601 (2019).

[16] Z. Wang and S.-C. Zhang, Simplified topological invariants for interacting insulators, Phys. Rev. X **2**, 031008 (2012).

[17] Z. Wang and B. Yan, Topological Hamiltonian as an exact tool for topological invariants, J. Phys.: Condens. Matter **25**, 155601 (2013).

[18] D. Lessnich, S. M. Winter, M. Iraola, M. G. Vergniory, and R. Valentí, Elementary band representations for the single-particle Green's function of interacting topological insulators, Phys. Rev. B **104**, 085116 (2021).

[19] M. O. Soldini, N. Astrakhantsev, M. Iraola, A. Tiwari, M. H. Fischer, R. Valentí, M. G. Vergniory, G. Wagner, and T. Neupert, Interacting topological quantum chemistry of Mott atomic limits, Phys. Rev. B **107**, 245145 (2023).

[20] H. H. Hu, L. Chen, C. Setty, M. Garcia-Diez, S. E. Grefe, X. Yan, M. Lužnik, N. Reumann, A. Prokofiev, S. Kirchner, M. G. Vergniory, S. Paschen, J. Cano, and Q. Si, Topological semimetals without quasiparticles, arXiv:2110.06182.

[21] L. Chen, C. Setty, H. Hu, M. G. Vergniory, S. E. Grefe, L. Fischer, X. Yan, G. Eguchi, A. Prokofiev, S. Paschen *et al.*, Topological semimetal driven by strong correlations and crystalline symmetry, Nat. Phys. **18**, 1341 (2022).

[22] H.-H. Lai, S. E. Grefe, S. Paschen, and Q. Si, Weyl-Kondo semimetal in heavy-Fermion systems, Proc. Natl. Acad. Sci. USA **115**, 93 (2018).

[23] S. Dzsaber, L. Prochaska, A. Sidorenko, G. Eguchi, R. Svagera, M. Waas, A. Prokofiev, Q. Si, and S. Paschen, Kondo insulator to semimetal transformation tuned by spin-orbit coupling, Phys. Rev. Lett. **118**, 246601 (2017).

[24] S. Dzsaber, X. Yan, M. Taupin, G. Eguchi, A. Prokofiev, T. Shiroka, P. Blaha, O. Rubel, S. E. Grefe, H.-H. Lai, Q. Si, and S. Paschen, Giant spontaneous Hall effect in a nonmagnetic Weyl Kondo semimetal, Proc. Natl. Acad. Sci. USA **118**, e2013386118 (2021).

[25] T. Morimoto and N. Nagaosa, Weyl Mott insulator, Sci. Rep. **6**, 1 (2016).
[26] A. A. Abrikosov, L. P. Gor'kov, and I. E. Dzyaloshinskii, *Methods of Quantum Field Theory in Statistical Physics* (Prentice-Hall, Englewood Cliffs, NJ, 1963).
[27] See the Supplemental Material at http://link.aps.org/supplemental/10.1103/PhysRevResearch.6.L032018 for details of the 2D and 3D models, their symmetries, and the Green's function methodology.
[28] S. M. Young and C. L. Kane, Dirac semimetals in two dimensions, Phys. Rev. Lett. **115**, 126803 (2015).
[29] Y. Hatsugai and M. Kohmoto, Exactly solvable model of correlated lattice electrons in any dimensions, J. Phys. Soc. Jpn. **61**, 2056 (1992).
[30] P. W. Phillips, C. Setty, and S. Zhang, Absence of a charge diffusion pole at finite energies in an exactly solvable interacting flat-band model in *d* dimensions, Phys. Rev. B **97**, 195102 (2018).
[31] C. Setty, Pairing instability on a Luttinger surface: A non-Fermi liquid to superconductor transition and its Sachdev-Ye-Kitaev dual, Phys. Rev. B **101**, 184506 (2020).
[32] C. Setty, Superconductivity from Luttinger surfaces: Emergent Sachdev-Ye-Kitaev physics with infinite-body interactions, Phys. Rev. B **103**, 014501 (2021).
[33] P. W. Phillips, L. Yeo, and E. W. Huang, Exact theory for superconductivity in a doped Mott insulator, Nat. Phys. **16**, 1175 (2020).
[34] E. W. Huang, G. L. Nave, and P. W. Phillips, Discrete symmetry breaking defines the Mott quartic fixed point, Nat. Phys. **18**, 511 (2022).
[35] K. Yang, Exactly solvable model of Fermi arcs and pseudogap, Phys. Rev. B **103**, 024529 (2021).
[36] H.-S. Zhu, Z. Li, Q. Han, and Z. D. Wang, Topological s-wave superconductors driven by electron correlation, Phys. Rev. B **103**, 024514 (2021).
[37] C. Setty, Dilute magnetic moments in an exactly solvable interacting host, arXiv:2105.15205.
[38] M. Fabrizio, Emergent quasiparticles at Luttinger surfaces, Nat. Commun. **13**, 1561 (2022).
[39] S. Raghu, X.-L. Qi, C. Honerkamp, and S.-C. Zhang, Topological Mott insulators, Phys. Rev. Lett. **100**, 156401 (2008).
[40] D. Sheng, Z.-C. Gu, K. Sun, and L Sheng, Fractional quantum Hall effect in the absence of Landau levels, Nat. Commun. **2**, 389 (2011).
[41] J. Kang and O. Vafek, Strong coupling phases of partially filled twisted bilayer graphene narrow bands, Phys. Rev. Lett. **122**, 246401 (2019).
[42] L. Fu, C. L. Kane, and E. J. Mele, Topological insulators in three dimensions, Phys. Rev. Lett. **98**, 106803 (2007).
[43] L. Fu and C. L. Kane, Topological insulators with inversion symmetry, Phys. Rev. B **76**, 045302 (2007).
[44] C. Setty, F. Xie, S. Sur, L. Chen, S. Paschen, M. G. Vergniory, J. Cano, and Q. Si, Topological diagnosis of strongly correlated electron systems, arXiv:2311.12031.
[45] C. Setty, F. Xie, S. Sur, L. Chen, M. G. Vergniory, and Q. Si, Electronic properties, correlated topology and Green's function zeros, arXiv:2309.14340.
[46] B. J. Wieder, Y. Kim, A. M. Rappe, and C. L. Kane, Double Dirac semimetals in three dimensions, Phys. Rev. Lett. **116**, 186402 (2016).
[47] B. Bradlyn, J. Cano, Z. Wang, M. G. Vergniory, C. Felser, R. J. Cava, and B. Andrei Bernevig, Beyond Dirac and Weyl Fermions: Unconventional quasiparticles in conventional crystals, Science **353**, aaf5037 (2016).
[48] D. Di Sante, A. Hausoel, P. Barone, J. M. Tomczak, G. Sangiovanni, and R. Thomale, Realizing double Dirac particles in the presence of electronic interactions, Phys. Rev. B **96**, 121106(R) (2017).
[49] A. Goldoni, U. del Pennino, F. Parmigiani, L. Sangaletti, and A. Revcolevschi, Electronic structure of Bi_2CuO_4, Phys. Rev. B **50**, 10435 (1994).
[50] J. L. Garcia-Munoz, J. Rodriguez-Carvajal, F. Sapina, M. J. Sanchis, R. Ibanez, and D. Beltran-Porter, Crystal and magnetic structures of Bi_2CuO_4, J. Phys.: Condens. Matter **2**, 2205 (1990).
[51] L. Chen, F. Xie, S. Sur, H. Hu, S. Paschen, J. Cano, and Q. Si, Emergent flat band and topological Kondo semimetal driven by orbital-selective correlations, Nat. Commun. **15**, 5242 (2024).
[52] H. Hu and Q. Si, Coupled topological flat and wide bands: Quasiparticle formation and destruction, Sci. Adv. **9**, eadg0028 (2023).
[53] L. Chen, F. Xie, S. Sur, H. Hu, S. Paschen, J. Cano, and Q. Si, Metallic quantum criticality enabled by flat bands in a kagome lattice, arXiv:2307.09431.
[54] N. Wagner, L. Crippa, A. Amaricci, P. Hansmann, M. Klett, E. J. König, T. Schäfer, D. D. Sante, J. Cano, A. J. Millis, A. Georges, and G. Sangiovanni, Mott insulators with boundary zeros, Nat. Commun. **14**, 7531 (2023).